metals

MDPI

Article

Correlation between the Liquid Fraction, Microstructure and Tensile Behaviors of 7075 Aluminum Alloy Processed by Recrystallization and Partial Remelting (RAP)

Jinlong Fu † , Dong Yang † and Kaikun Wang *

School of Materials Science and Engineering, University of Science and Technology Beijing, Beijing 100083, China; jinlongsjz@126.com (J.F.); yd.ustb@foxmail.com (D.Y.)

* Correspondence: kkwang@mater.ustb.edu.cn; Tel.: +86-1-6233-3892

† These authors contributed equally to this work.

Received: 4 June 2018; Accepted: 21 June 2018; Published: 2 July 2018

Abstract: The recrystallization and partial remelting (RAP) method was applied to obtain the semisolid 7075 aluminum alloy with different liquid fractions. The effects of liquid fraction on the microstructure and tensile properties were determined in detail. The results show that during the semisolid isothermal treatment, the number of the intra-granular liquid droplets increased initially with the melting of the eutectic phases. Extension of isothermal soaking led to the coarsening and spheroidization of the intra-granular droplets. Finally, these liquid droplets merged and moved towards the grain exterior. The room temperature tensile strength of the RAP-processed AA7075 alloy, which were isothermally soaked at 600 and 610 °C, increased with the holding time from 5 to 15 min and then decreased dramatically from 15 to 25 min, whilst that soaked at 620 °C decreased monotonously. The fracture morphology exhibited intra-granular fracture mode at low liquid fractions. However, it transformed to a completely brittle and inter-granular type at high liquid fractions and the cohesive force of the liquid-solid interfaces at the grain boundaries determined the strength of the alloys. The transfer of the intra-granular liquid droplets into the inter-granular liquid phase played a significant role for the different fracture behaviors of the RAP-processed AA7075 alloy. The paper provides some reference for better controlling the microstructure and mechanical properties in semisolid processing.

Keywords: aluminum; liquid droplets; tensile properties; semisolid; fracture mechanisms

1. Introduction

Semisolid processing (SSP) supplies an effective near-net shape-forming method for the steels [1,2] and nonferrous alloys [3–5] and composites [6,7]. It has already been proved that both thixoforming and rheoforming provide the components with excellent forming ability and considerable mechanical properties [8,9]. Particularly, the mechanical properties of the thixoformed components are close to the forged ones [10–12]. Slurry or feedstock with spherical grains and uniform liquid film is essential for obtaining thixotropic behavior in the semisolid state [13]. Recrystallization and partial remelting (RAP) is one of the most promising routes for fabrication of the semisolid feedstock and slurry. The RAP process involves the warm working of the materials below the recrystallization temperature and subsequent reheating to the semisolid temperature range to obtain the equiaxed grains surrounded by the liquid phase.

It is believed that the RAP route could produce finer semisolid microstructure and significantly advantageous mechanical properties compared with semisolid thermal transformation (SSTT)

route [14]. The semisolid microstructure is largely determined by the plastic deformation and subsequent partial remelting processes [8,9]. Campo et al. [15] prepared the semisolid A356 alloy through five different processing routes and suggested that the material deformed by an equal channel angular pressing (ECAP) before partial remelting presented the most suitable characteristics for thixoforming, e.g., smaller grain size and greater sphericity. Nayyeri and Dehghani [16] and Bolouri et al. [17,18] investigated the influences of compression ratio on the semisolid microstructure and declared that the average grain size was gradually decreased with the increment of the compression ratio by the increased accumulated strain energy. In addition, it was found that during the semisolid isothermal treatment (SSIT), higher soaking temperatures and longer holding time accounted for larger and spheroidal grains in the semisolid microstructure [19–21].

Furthermore, the tensile properties of the SSP-formed samples are greatly linked to the corresponding semisolid microstructure. It has been reported that the room temperature tensile properties of aluminum alloys processed by RAP show a significant improvement over mold casting but lower than those of as-extruded ones [12,22]. Bolouri et al. [23] investigated the effects of liquid fractions on the room temperature tensile properties of AA2024, AA6061, and A356 aluminum alloys by RAP route. The results showed that the increase of the liquid fractions resulted in an initial reduction followed by an improvement of the tensile strength. The paper declared that the fracture mechanism depended on the liquid fractions, and the weakening effect of the interconnected grains was presumed to be the reason for the lower strength for the SSP samples. Jiang et al. [10] found that the tensile strength of the thixoformed products decreased slightly with the increasing isothermal temperatures. Arami et al. [20] found that the ultimate tensile strength of 319 aluminum alloy increased to a maximum value and then decreased to lower values when holding at 580 °C for 0 to 40 min. The author claimed that this decrease was related to the excess coarsening of the solid grains. However, the fracture mechanisms of the tensile samples with different holding time were not investigated in the paper.

As the ultra-high strength wrought aluminum series, Al–Zn–Mg–Cu aluminum alloys have already been applied in the fields of aerospace and automobiles. SSP provides an alternative route for the Al–Zn–Mg–Cu alloys. The mechanical properties of the SSP-processed samples are generally dominated by the liquid fractions within the microstructure. In practical manufacturing, the volume fraction of liquid phase within the microstructure varies not only with the isothermal temperatures, it also changes with the isothermal soaking time. The latter issue is because the existence of intra-granular liquid droplets remarkably reduces the effective liquid fraction, i.e., inter-granular liquid fraction, in the microstructure and thus the semisolid alloy exhibits distinctly different tensile behaviors with the isothermal soaking time. However, there is lack of the elaborate reference about the effects of isothermal holding time on the tensile strength and fracture mechanisms of AA7075 alloy. In this paper, two key factors that influence the liquid fractions, namely isothermal temperatures and soaking time, were examined and linked to the corresponding semisolid microstructure and room temperature (RT) tensile properties of RAP-processed AA7075 alloy. The evolution of the intra-granular liquid droplets in the semisolid microstructure were also discussed. The aim of present paper is to provide some reference on the relations between the processing parameters and tensile behaviors for the aluminum alloys.

2. Materials and Methods

Commercial 7075-T6 aluminum alloy was used as the initial material, and the chemical composition was 6.05 wt. % Zn, 2.48 wt. % Mg, 1.63 wt. % Cu, 0.24 wt. % Fe, 0.15 wt. % Si, 0.23 wt. % Cr, 0.39 wt. % Mn and balance of Al. The heat flow–temperature relationship was determined by differential scanning calorimeter (DSC, SDT-Q600). Sample of the as-received material (15 mg) was put into the alumina pan and then heated to 700 °C at 10 °C/min under nitrogen atmosphere. The curve of liquid fraction versus temperature was determined by integrating the obtained DSC curve. X-ray diffraction (XRD) was carried out using a Smartlab 9 KW model apparatus with Cu (Kα) target and wavelength of 0.15406 nm.

As the initial materials had already been deformed with the extrusion ratio of about 16:1, the as-received alloys were directly soaked at 600 °C, 610 °C, and 620 °C for 5 to 25 min in an electric resistance furnace. Immediately after the samples were soaked for the required time, they were quenched into warm water (60 °C) for at least 30 s to freeze the microstructure.

The specimens were cut from the quenched samples parallel to the extrusion direction. The RT tensile test were performed using WDW-200D tensile testing machine, and the strain rate was 10^{-3} s^{-1}. The tensile curves were analyzed to assess the ultimate tensile strength (UTS), yield tensile strength (YTS), and elongation to failure (EL). The measured UTS, YTS, and EL values were the average results of three test specimens. The fracture samples were sectioned and prepared through the standard metallographic technology. Both the morphologies of profiles of the fractures and the fracture surfaces were examined by the optical microscope (OM, German Zeiss-Imager M2) and scanning electron microscope (SEM, German Zeiss EVO-18) equipped with energy dispersive spectrometer (EDS). The average grain size was defined as $D = (4\ A/\pi)^{1/2}$, where D and A represent the size and area, respectively. The shape factor was defined as $F_S = P^2/(4\pi A)$, where P is the perimeter of the grain. Over 300 solid grains were measured for each sample.

3. Results and Discussion

3.1. Effects of Liquid Fractions on the Microstructural Evolution

Figure 1a shows the DSC curve and the relationship between liquid fraction and reheating temperature is shown in Figure 1b. The solidus and liquidus temperatures were about 482 °C and 652 °C, respectively. The theoretical volume fraction of liquid phase at 600 °C, 610 °C, and 620 °C were 17%, 22%, and 37%, respectively.

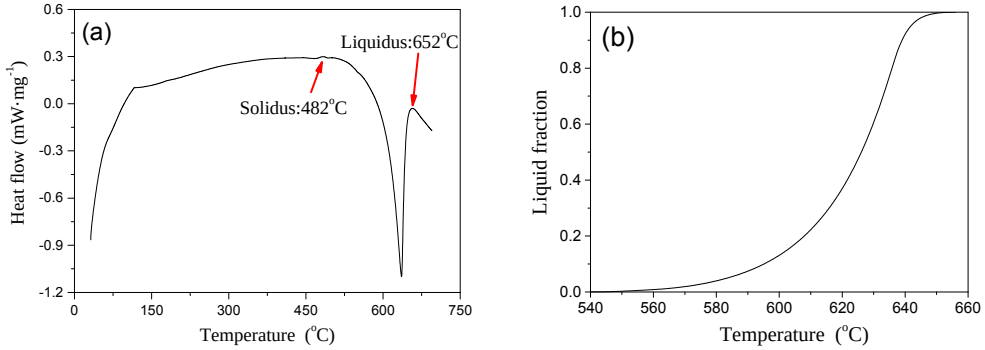

Figure 1. DSC curve (**a**) and the variation of liquid fraction versus heating temperature (**b**) of AA7075 alloy.

Figure 2 shows the OM images of the AA7075 samples soaked at 600–620 °C for 5–25 min. The corresponding quantitative results of the average grain size and the shape factor are shown in Figure 3. Obviously, the general trend of the average size and the shape factor increased with the higher temperatures and prolonged holding time, which was also proved by ref. [19–21]. The evolution of the microstructure in the semisolid state is actually a process of atom diffusion, and the liquid phase in the microstructure provides a much faster diffusion path for the alloying elements. Higher soaking temperature and prolonged holding time promote the diffusion evolution by accelerating the volume fractions of the liquid phase.

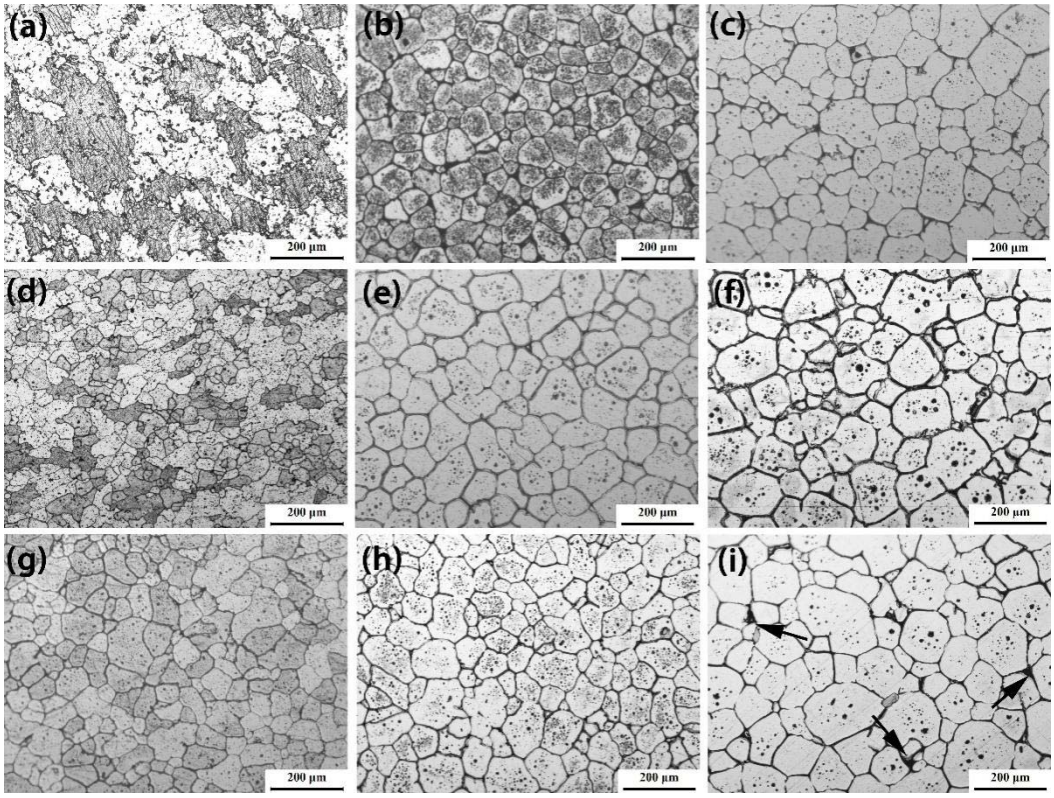

Figure 2. The OM images of the recrystallization and partial remelting (RAP)-processed AA7075 alloy held at 600–620 °C for 5–25 min, (**a**) 600 °C-5 min; (**b**) 600 °C-15 min; (**c**) 600 °C-25 min; (**d**) 610 °C-5 min; (**e**) 610 °C-15 min; (**f**) 610 °C-25 min; (**g**) 620 °C-5 min; (**h**) 620 °C-15 min; (**i**) 620 °C-25 min.

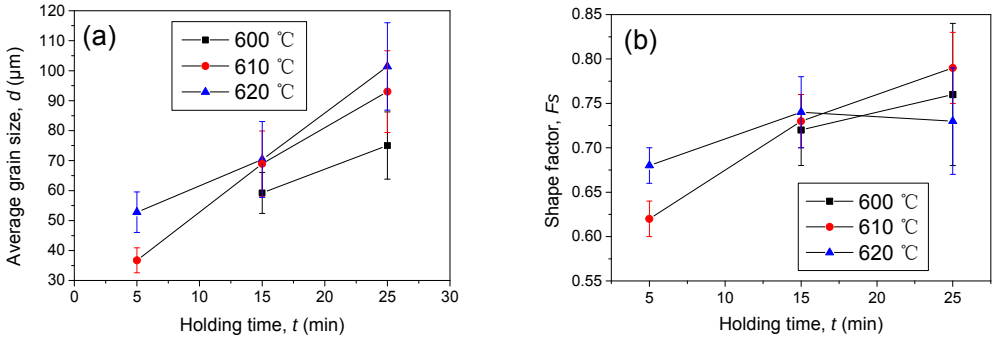

Figure 3. The quantitative results of the average grain size (**a**) and shape factor (**b**) of the RAP-processed AA7075 alloy that soaked at 600–620 °C for 5–25 min.

According to Figure 2, the microstructural evolution in the semisolid temperature range can be divided into three stages: (I) recrystallization and grain separation, (II) coarsening and spheroidization, and (III) grain polygonization. The final size and shape of solid grains in the semisolid microstructure is the balance of coarsening, spheroidization, and dissolution. In fact, AA7075 alloy is difficult to recrystallize in the solid state due to the existence of dispersed intermetallic particles like E-phase [24]. These particles hinder the migration of the grain boundaries and will not melt before being wetted by the liquid phase. Therefore, the recrystallization occurs only after the formation of the adequate liquid in the microstructure. For the sample held at 600 °C for 5 min, the recrystallization was not completed and initial deformed grains could be observed (Figure 2a). Soaking the sample at 610 °C for 5 min (Figure 2d), nearly all the grains completed the recrystallization process and the microstructure

contained fine and equiaxed grains. Reheating the sample at 620 °C for 5 min (Figure 2g), the liquid phase started to separate the grain boundaries, and the solid grains coarsened slightly. As soon as the formation of the liquid film at the grain boundaries, grain coarsening, and spheroidization became the main microstructural change during the semisolid soaking, the result was the increase of the average size and the sphericity of the solid grains, as can be indicated in Figure 3. However, if the sample was soaked at higher temperatures (e.g., 620 °C) for an excessively long time (e.g., 25 min), the grain boundaries became polygonal and faceted, and this led to a reduction of the roundness of the solid particles, as shown in Figure 3b. Additionally, some quenched liquid pools located at the junction regions of three or more grains were indicated by the arrows in Figure 2i. The segregation of the liquid phase as well as the polygonization of the solid particles deteriorated the thixotropic characteristic of the RAP-processed samples, and therefore, excessive isothermal semisolid holding should be avoided.

Additionally, some quenched in-grain liquid droplets could be observed in Figure 2. Due to the occurrence of these liquid droplets, the liquid fraction was lower than the theory value in Figure 1b. Meanwhile, the mobility of these intra-granular droplets was much lower than that of the inter-granular liquid film. These intra-granular droplets could hardly contribute to the atomic diffusion during grain-coarsening and spheroidization. Therefore, the rate of microstructural evolution was hindered. In this regard, the intra-granular droplets have significant influence on the microstructural evolution and tensile properties of RAP-processed AA7075 alloys.

3.2. Formation of Liquid Phase and Evolution of Intra-Granular Liquid Droplets during SSIT

The SEM images of the quenched AA7075 samples after soaking at 610 °C for various times are shown in Figure 4. For the specimen held at 610 °C for 5 min, some intermetallic particles start to melt at the areas where a high volume fraction of alloying elements is concentrated (as indicated in white arrows in Figure 4a. According to Binesh and Khafri [25,26], when the heating temperature reached above the solidus temperature, η-$MgZn_2$, θ-Al_2Cu and Mg_2Si started to melt and transformed to the liquid phase by reacting with Al. Mostly, the formed liquid phases were interconnected and distributed at the grain boundaries, whereas a few large liquid pools could be found at triple junctions among the solid grains as well as within the grains. These intra-granular droplets usually appeared as clusters in the centers of grains or in the form of rings [27,28]. The existence of these intra-granular droplets greatly reduces the "effective" or "active" liquid phase (inter-granular liquid film) in the semisolid microstructure and thus decreases the rate of microstructural evolution. However, because of insufficient soaking period, no continuous liquid films were formed, and some insoluble particles could be found in Figure 4a. Following soaking the sample to 10 min, the volume fraction of the quenched intra-granular liquid droplets and inter-granular liquid phase increased remarkably. The liquid film would replace the grain boundaries when the surface energy of the grain boundaries was greater than two fold of solid/liquid interfacial energy [29]. The majority of the grain boundaries were wetted by the liquid film while small parts of them were still connected by solid–solid necks. In addition, most of the quenched intra-granular liquid droplets appeared to have coarsened slightly compared to that of holding for 5 min. Further extension of holding time to 15–25 min, the liquid fraction further increased, and the interconnected liquid network was formed at the grain boundaries. In Figure 4d, abnormal large grains were formed by the coalescence of two neighborhood solid grains (as indicated by the white arrow). It is worth noting that the occurrence of several small grains indicated that some of the grains grew through the Ostwald ripening mechanism. For the sample held for 25 min, the number of the intra-granular droplets evidently decreased. Almost each grain contained a droplet-depleted zone at the peripheral region, and this indicated the expansion of the grain boundaries during the grain coarsening [27]. Considering the sample that held for 30 min (Figure 4f), solid grains were apparently coarsened and became more spherical. The quenched liquid droplets were gradually attached to the grain boundaries. Some droplet-depleted grains marked G1 and G2 could be observed while others owned very limited number of liquid droplets, e.g., grains marked G3 and G4.

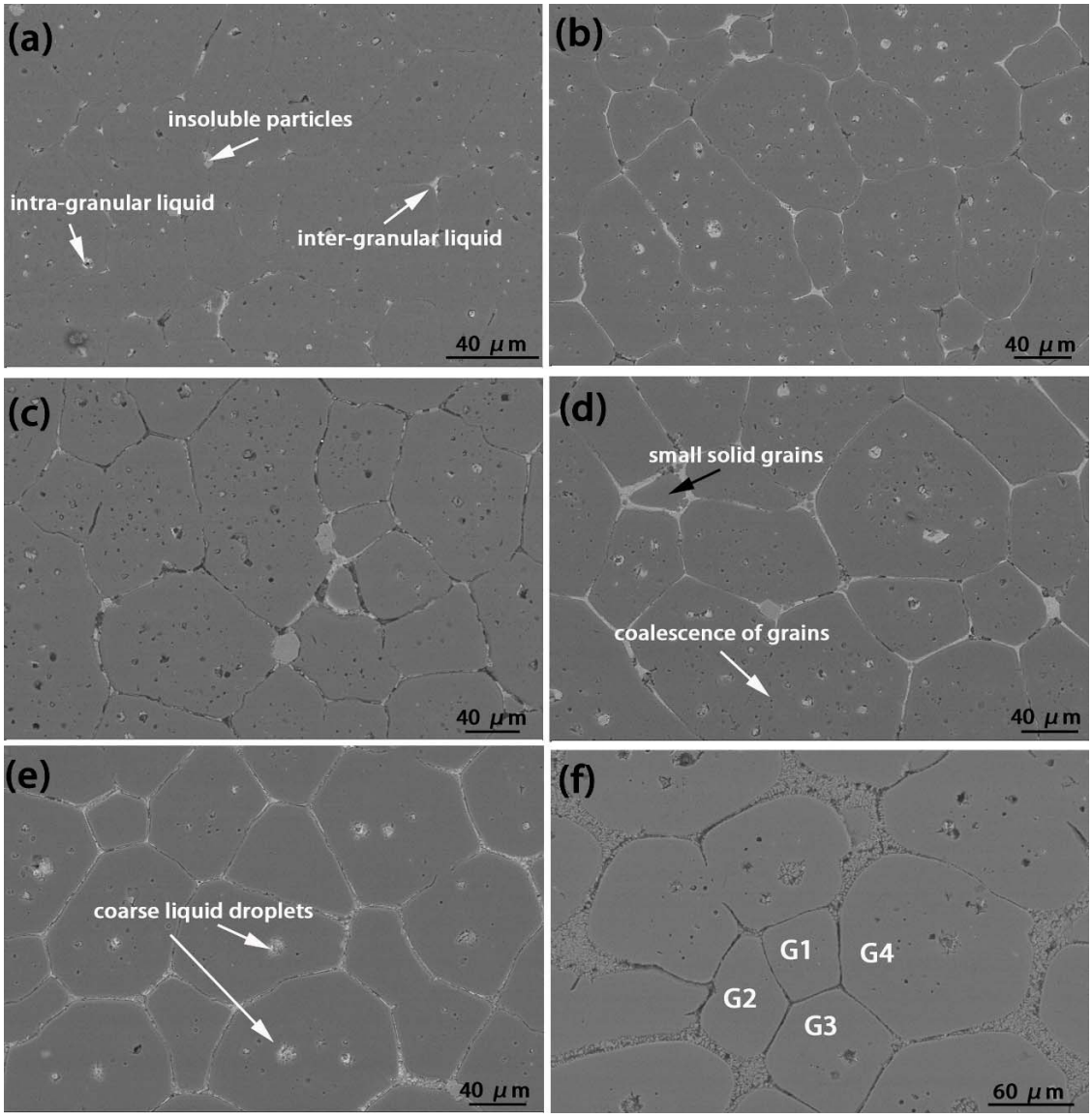

Figure 4. SEM images of the RAP samples after soaked at 610 °C for (**a**) 5 min; (**b**) 10 min; (**c**) 15 min; (**d**) 20 min; (**e**) 25 min and (**f**) 30 min.

Figure 5 shows the SEM images and corresponding EDS patterns of the AA7075 samples that held at 620 °C for 10 min. In Figure 5a,b, large amounts of intra-granular liquid droplets can be found within the solid grains, while inter-granular liquid film is located at the grain boundaries. According to the EDS analysis shown in Figure 5c, the solid grains are the Al matrix with some Al atoms being substituted by Mg and Zn, which can be proved in aluminum-related reviews [30–32]. Based on Figure 5d,e, the quenched in-grain and inter-grain liquid exhibited similar chemical composition; it can be deduced that both kinds of liquid phase were derived from the re-melting of the eutectic structure in AA7075 alloy after casting. During the plastic deformation and heat treatment, the interdendritic eutectic phase evolved into the liquid film at the grain boundaries while the dendritic arms within the grains coalesced, trapping the eutectic between the dendritic arms as isolated droplets. The main source of the intra-granular liquid droplets came from the inhomogeneous distribution of the eutectic phase during the evolution of the dendritic structure, as indicated in Figure 5a.

In addition, the grain coalescence in the early stage of the SSIT also promoted the formation of the intra-granular droplets. For instance, as shown in Figure 5f, the grain boundaries migrated, merged,

and were detached from the coarsened grains. The liquid film located at the grain boundaries initially were gradually enclosed by the coarsened solid grains, and then the liquid became isolated droplets. This phenomenon can be also certified by Chen et al. [33] and Jiang et al. [34].

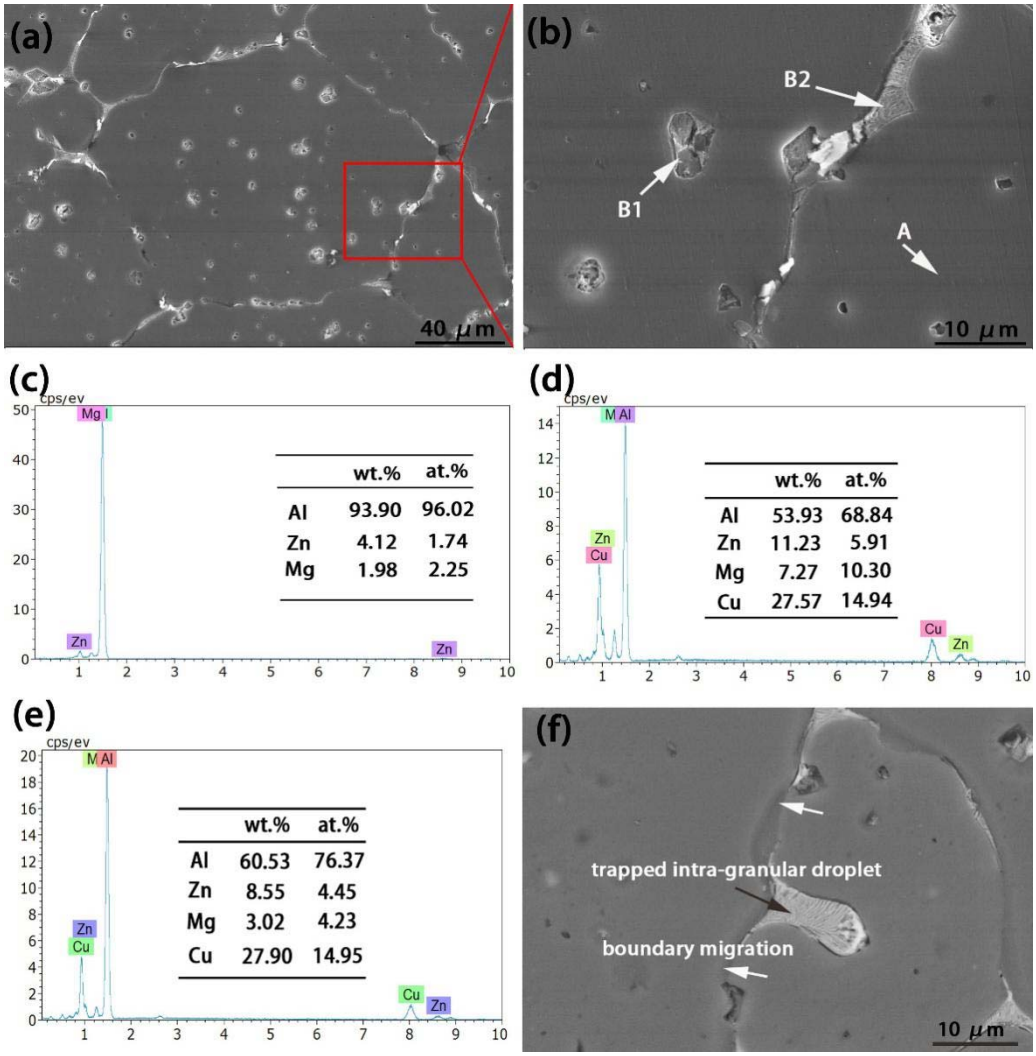

Figure 5. The SEM microstructure and corresponding EDS patterns of RAP-processed samples soaked at 620 °C for 10 min, (**a**) low magnification; (**b**) high magnification; (**c**) EDS patterns of points A in (**b**); (**d**) EDS patterns of points B1 in (**b**); (**e**) EDS patterns of points B2 in (**b**); (**f**) migration of grain boundaries.

The intra-granular droplets also experienced the coarsening and spheroidization processes during the SSIT, as that of the grains did. Figure 6 shows the SEM images of the RAP-processed AA7075 alloy held at 620 °C for 15 min. In Figure 6a, some liquid droplets with similar size, as shown in arrow C1 and C2, were merging into a larger liquid pocket. Meanwhile, some smaller liquid droplets were absorbed in a larger one, as indicated in arrow D. Irregular and coarse quench liquid droplets could be found at arrow E in Figure 6a. The size of the coarsened liquid droplets ranged from several hundreds of nanometers to about 10 μm. In order to reduce the liquid–solid interfacial energy of the semisolid system, the liquid droplets move gradually toward the grain boundaries, as shown by the arrow in Figure 6b. Finally, the liquid droplets were attached to the grain boundaries and then released to the liquid film at the grain boundaries.

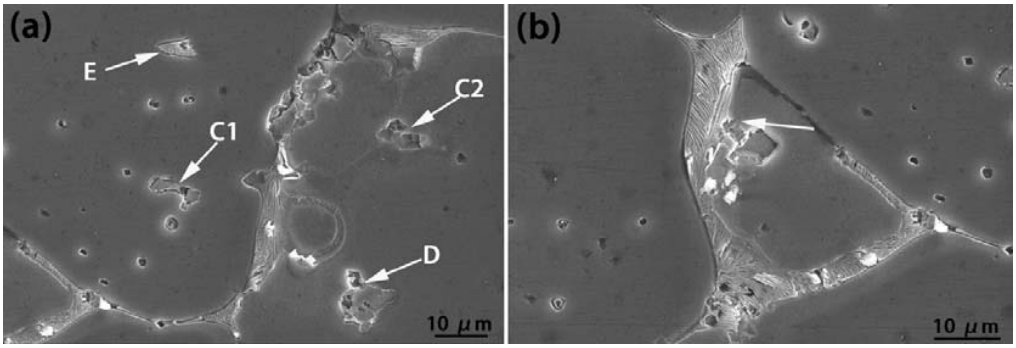

Figure 6. The SEM images of the RAP-processed AA7075 alloy held at 620 °C for 15 min, the process of coarsening (**a**) and migration (**b**) of the intra-granular liquid droplets.

In general, the liquid migration mechanism is driven through descending the interfacial energy. As shown in Figure 7a, six stages can be classified to describe the intra-granular liquid migration process with the increasing isothermal time: the distribution of eutectic phase and alloying elements in the solid state is schematically plotted in stage (I). When the temperature was above the solidus, the eutectic phases started to melt, and the liquid phase formed, as shown in stage (II). In stage (III), the droplets began to grow through the coarsening and spheroidization. As the soaking time was increased, the solid grains grew larger and the droplets' depleted area occurred in the edge region of the grains, as shown in stage (IV). In stage (V), the coarsened liquid droplets began to move to the grain boundaries in order to reduce the solid–liquid interface energy. Finally in stage (VI), the liquid droplets were expelled out of the grains and flew into the liquid films at the grain boundaries. The depletion of the alloying elements within the grains increased the melting point of the solid grains whereas the liquid films at the grain boundaries became thicker.

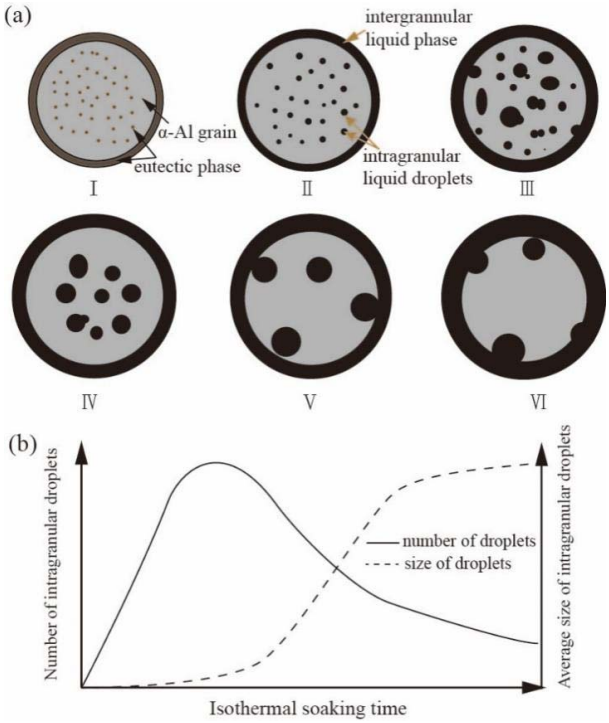

Figure 7. The evolution of intra-granular liquid droplets, (**a**) schematic illustration of the evolution of intra-granular droplets; (**b**) the variation of the number and average size of the intra-granular liquid droplets during SSIT.

For the above analysis, the variation of the number and average size of the intra-granular liquid droplets are shown in Figure 7b. The number of intra-granular liquid droplets increased rapidly in the initial stage of SSIT and then reduced gradually, which was linked to the formation and coarsening processes, respectively. Meanwhile, the average size of these droplets increased monotonously, as could be examined by Figure 2.

3.3. Effects of Liquid Fractions on the Room Temperature Tensile Properties

The tensile properties of the semisolid components are affected by the grain size, liquid fraction, and sphericity of the solid grains [35,36]. Fine and equiaxed grains are generally preferable because they provide the best combination of the strength and ductility by maximizing the grain boundary surface area and more finely distributing the grain boundary constituents [20]. However, according to the earlier discussion in the present study, the average grain size has a strong dependence on the liquid fractions, and it is difficult to distinguish the individual influence on the tensile properties. Therefore, only the influence of the liquid fractions on the tensile properties of AA7075 alloy will be discussed in present study.

Figure 8 shows the representative stress–strain curves and corresponding UTS, YTS, and EL of the quenched AA7075 alloys with different heating temperatures and isothermal holding time. According to Figure 8, for the samples that soaked at 600 and 610 °C, the UTS and YTS experienced an increase for the first 15 min followed by a reduction for 15–25 min. However, the UTS and YTS that heated at 620 °C decreased with the holding time. Moreover, the UTS and YTS values for the samples that held for the same period decreased with the increasing heating temperatures. For all the test samples, the EL decreased with the temperatures and holding time. Particularly, the samples after soaking at 620 °C could hardly stand any strain and exhibited typical brittle behavior.

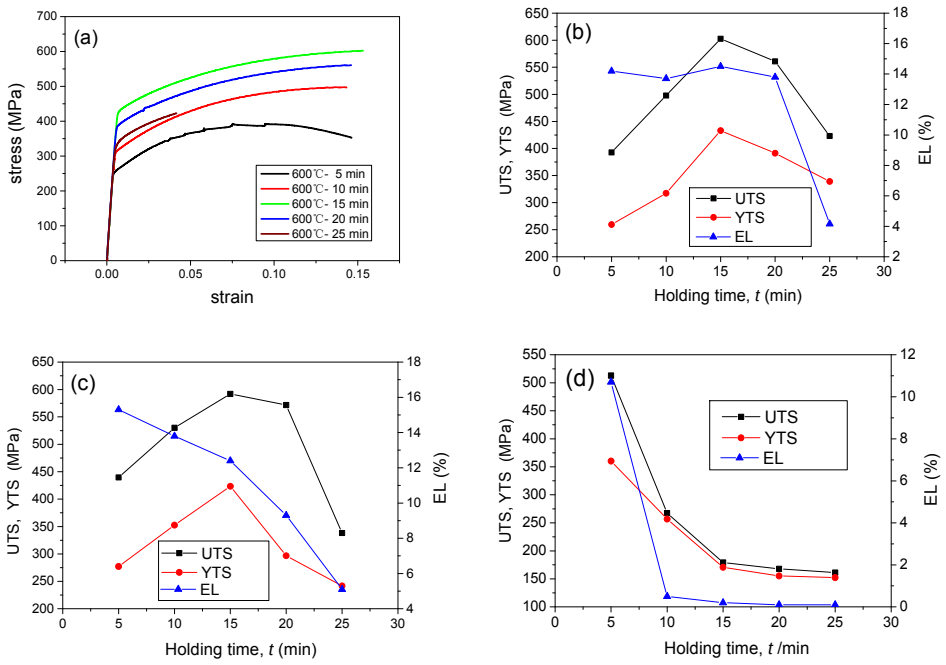

Figure 8. (**a**) The representative stress–strain curves of the RAP-processed samples soaked at 600 °C for 5–25 min and the ultimate tensile strength, yield strength, and elongation versus temperatures and holding time of the RAP-processed 7075 aluminum alloy, (**b**) 600 °C; (**c**) 610 °C; (**d**) 620 °C.

Figure 9 shows the SEM images of the fracture surfaces and profiles (side views) of the room temperature tensile specimens after soaking at 620 °C for 5 min. The fracture surfaces of the tensile samples exhibited a mixture mode of ductile and brittle with the evidence of larger fractions of small

dimples and some cleavage planes (Figure 9a,b). In Figure 9c,d, the intra-granular fracture, as indicated by the arrows, was the main fracture type for this microstructure. Micro-pores were observed near the fracture surfaces in the microstructure. Due to the low liquid fractions, the strength was less influenced by the liquid phase but largely determined by the solid phase.

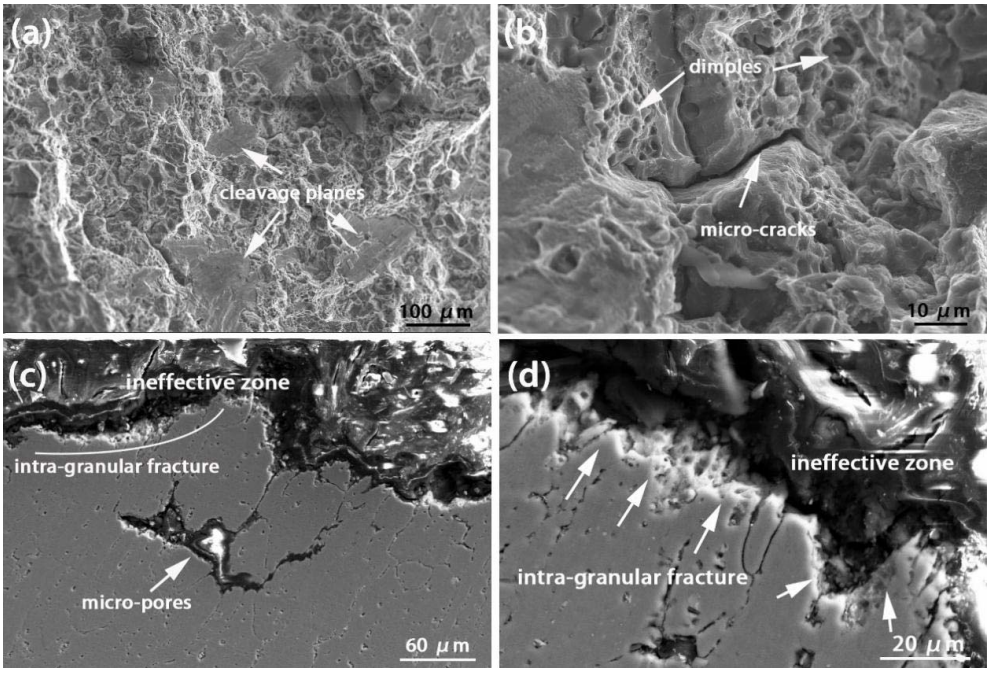

Figure 9. SEM images of the fracture morphology of the RT tensile samples that soaked at 620 °C for 5 min, (**a**,**b**) fracture surfaces; (**c**,**d**) fracture profiles.

For the samples that soaked for 15 min at 620 °C, as indicated in Figure 10a, the grains became more spherical and the fracture mode transformed into the inter-granular type. The shearing effect under the tensile stress loosened the strength between the grains, and the surrounding liquid phase and resulted in decohesion between the grains' necks marked "F" and "G". Many micro-pores were found at the triple junctions of the grains, as shown in Figure 10b. It can be concluded that during the solidification, because of the simultaneous effects of the solidification shrinkage and the absence of the liquid feeding to the liquid film at the grain boundaries, especially for the lower cooling rate, the liquid films lost their interfacial bonding force with the solid grains and cracks might occur along the grain boundaries. These micro-pores and micro-shrinkage rapidly propagated under the tensile stress and finally resulted in the failure of the materials.

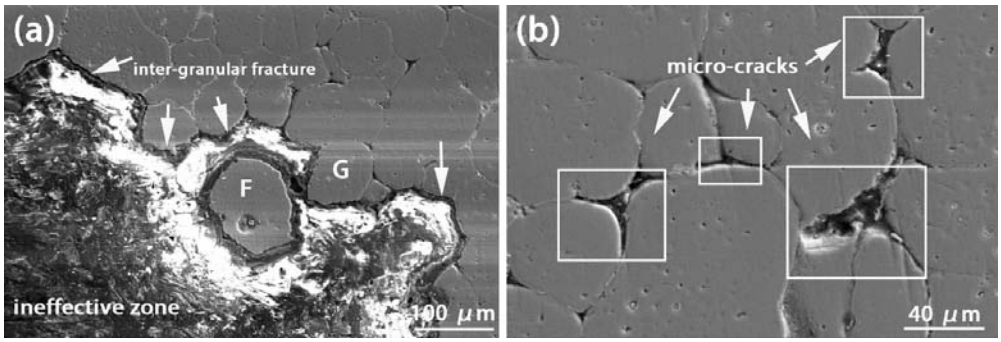

Figure 10. The SEM images of the fracture profiles of the room temperature tensile samples that soaked at 620 °C for 15 min, (**a**) low magnification; (**b**) high magnification.

Additionally, the insoluble intermetallic compounds located at the grain boundaries easily caused the stress concentration during the tensile test. Due to their low fractions, coarse intermetallic compounds have relatively little effect on yield or tensile strength but can cause a marked loss of ductility [21]. Therefore, continuous reduction of the elongation can be observed in Figure 8.

For the samples with higher liquid fractions (higher temperatures and adequate holding time), most of the intermetallic particles were dissolved into the liquid phase. The intra-granular liquid droplets are released to the liquid pools at the grain boundaries and increased the volume fraction of the inter-granular liquid. Additionally, higher liquid fraction provided the adequate liquid feeding and therefore decreased the frequency of the shrinkage and cracks during the solidification from the semisolid temperature. The deteriorate effects of the micro-porosity and the intermetallic compounds on the tensile properties became insignificant. Different fracture mechanism, presumably, occurred in the microstructure linking to the higher liquid fractions.

For the samples that soaked at 620 °C for 25 min, the fracture mode transformed into the typical brittle with the evidence of the inter-granular fracture morphology, as indicated in Figure 11a,b. In Figure 11c,d, the solid grains almost maintained spherical and no obvious plastic deformation was found. Solid grains were loosely interconnected and formed a structure skeleton. The liquid fraction increased noticeably since large amounts of the intra-granular droplets were supplied to the liquid films at the grain boundaries. Micro-cracks occurred mainly along the grain boundaries. Obviously, the liquid phase plays an important role in determining the strength of the RAP-processed samples under this condition.

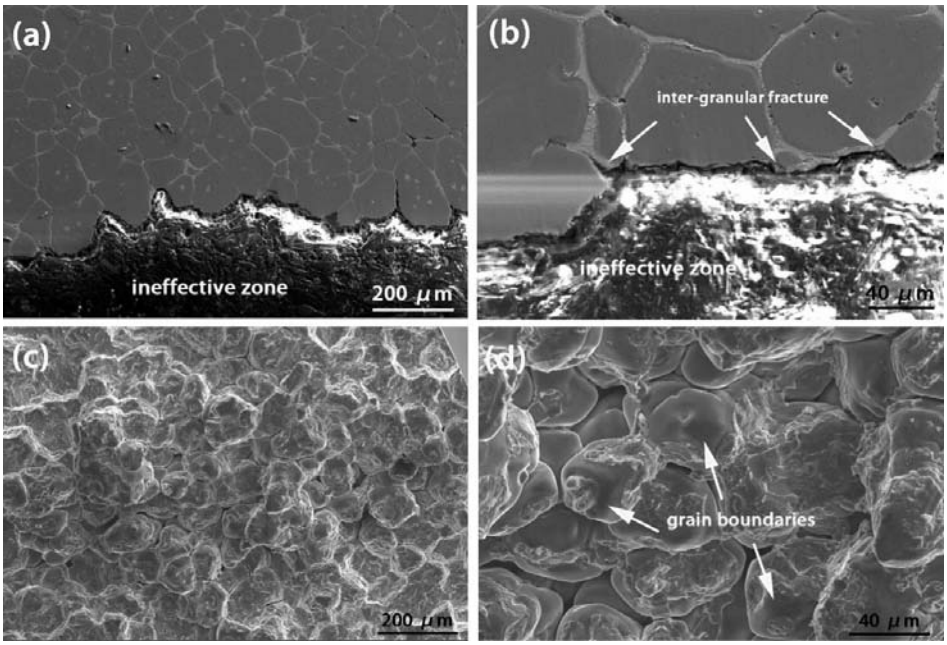

Figure 11. SEM images of the fracture micrographs of the room temperature tensile samples after reheating at 620 °C for 25 min, (**a**,**b**) fracture profiles; (**c**,**d**) fracture surfaces.

Further detailed inspection of the fracture surfaces for high liquid fractions, as shown in Figure 12a,b, indicated that two typical types of the inter-granular fractures can be classified: (I) decohesion through the quenched liquid film located at the grain boundaries and (II) decohesion at the interfaces between the solid grains and the quenched liquid phase. Higher magnification images of the two decohesion types can be found in Figure 12c,d, marked by arrow α and β. In other words, the cohesion strength of the quenched liquid phase as well as the interface between the quenched liquid film and the solid grains determined the tensile strength of the RAP-processed AA7075 alloy [20]. Bolouri et al. [23] described the schematic illustration of these two typical decohesion types and was

illustrated in Figure 12e. The bonding force of the interface between the grains and quenched liquid phase have a dominant effect on the tensile strength fracture behavior of RAP-processed alloys for the high liquid fractions. Unfortunately, the bonding strength of the liquid phase or that between the eutectic phase and solid grains are usually much weaker than the intrinsic strength of the solid materials, thus the occurrence of the liquid film results in the reduction of the strength of the semisolid materials, and it is usually difficult to eliminate this effect even after heat treatment. Therefore, the strength of the RAP-processed samples is believed, theoretically, to decrease with the prolonged holding time.

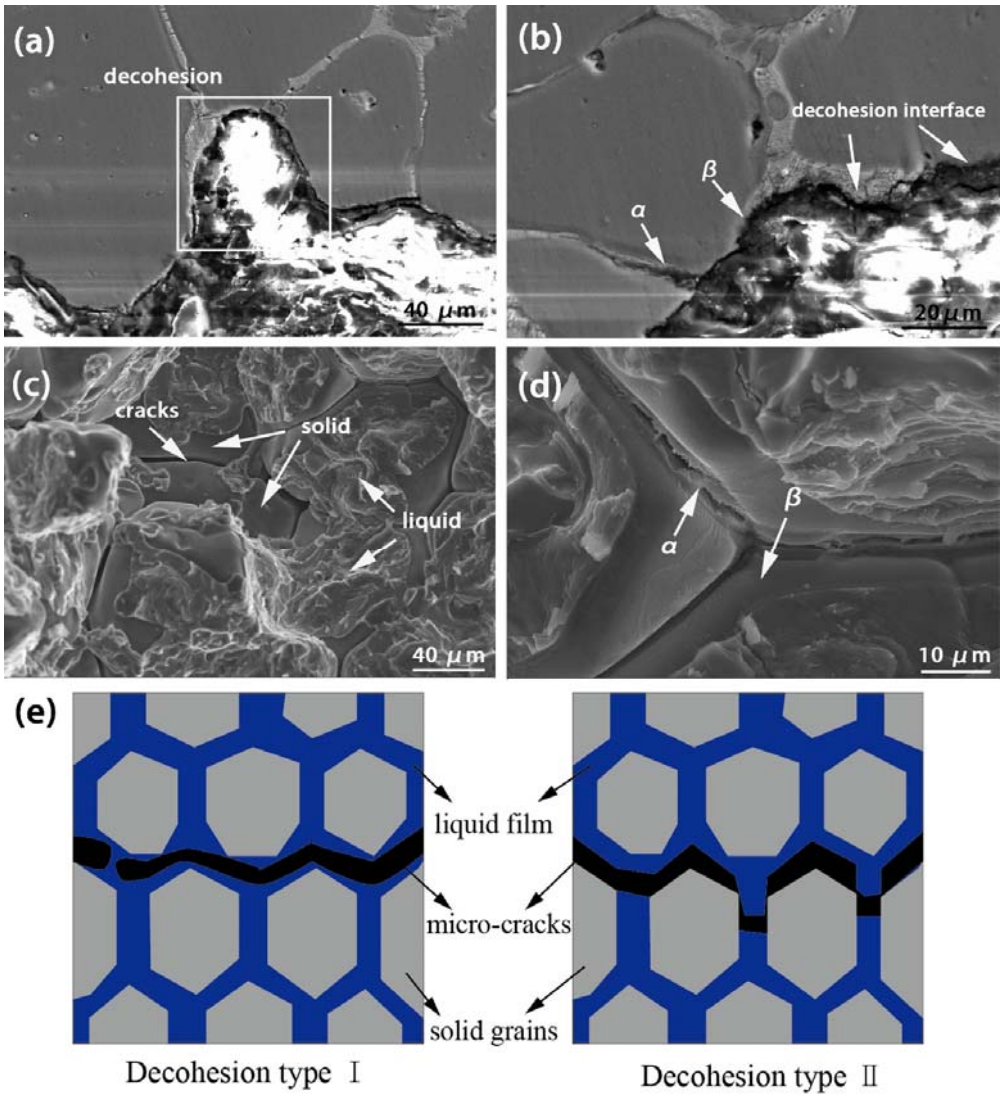

Figure 12. The SEM image of (**a**,**b**) fracture profiles and (**c**,**d**) fracture surfaces of the RAP-processed AA7075 alloy after reheating at 620 °C for 25 min; (**e**) The schematic illustration of two kinds of decohesion types (by Bolouri et al. [23]).

However, from Figure 8b,c, UTS and YTS of the samples that soaked at 600 °C and 610 °C increased with the holding time for the initial 15 min. Two possible reasons account for this interesting phenomenon. Firstly, for the short holding time of the SSIT, some of the grains were connected with each other and a neck formed by the migration of the boundaries because of the low liquid fractions, as shown in Figure 13a. With the increase of the holding time, an obvious increase of the size of the neck could be found (Figure 13b). German et al. [37] found that the neck grows simultaneously and

proportionally with the solid grains. A larger neck size usually promotes a higher strength during the deformation and thus contributes to a higher cohesion force for the semisolid samples. Secondly, for the samples soaked at 600 °C and 610 °C for 5–15 min, the increased volume fraction of liquid decreases the micro-shrinkage and micro-pores, which is detrimental to the strength of the samples. Therefore, for the samples heating at 600 and 610 °C for 5–15 min, an increase of the strength of the UTS and YTS could be found. However, with the increment of the isothermal holding time in the semisolid temperature range, the liquid fractions increased dramatically and the necks were wetted by the liquid phase or disappeared during the coarsening process, as can be verified in Figure 4. Correspondingly, the tensile properties of the RAP-processed alloys were independent of the presence of neck structure.

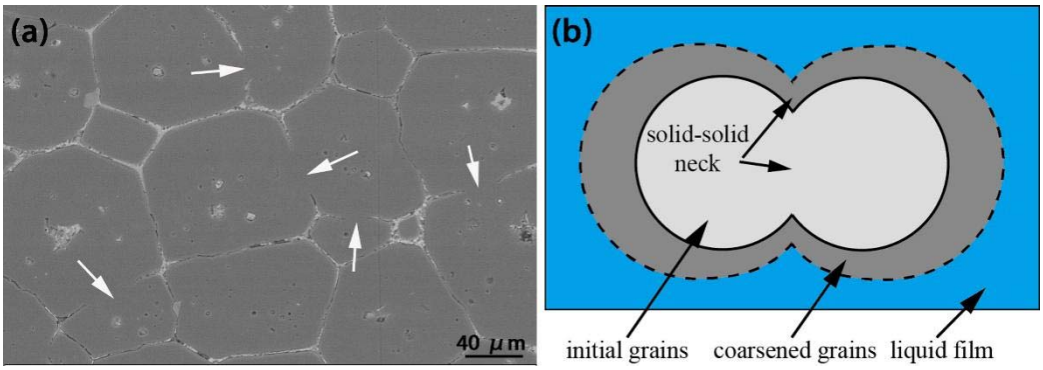

Figure 13. SEM image of the sample soaked at 610 °C for 10 min (**a**) and schematic illustration (**b**) of the coarsening of the solid–solid neck during the SSIT.

4. Conclusions

In present study, AA7075 alloy was prepared by the RAP route, and the tensile experiments of the semisolid samples with different liquid fractions were carried out. The following conclusion can be drawn from the above results and analysis.

The deformed microstructure experiences the recrystallization, liquid penetration, coarsening and globularization process during the isothermal holding in the semisolid temperature range. The volume fraction of the liquid phase in the semisolid microstructure increases with the increasing temperatures and prolongs holding time. Higher heating temperatures accelerate the rate of microstructural evolution.

The occurrence of the intra-granular liquid droplets reduces the volume fractions of the inter-granular liquid, and the rate of microstructural evolution is decreased. With the increment of isothermal soaking time, intra-granular liquid droplets are transformed into the inter-granular liquid phase, thus promoting the "effective" liquid fractions in the semisolid microstructure.

For the low liquid fractions, the fracture mode of the quenched RAP processed sample is a mixture of ductile and brittle, while it turns to completely brittle mode when the liquid fraction is high. When the liquid fraction is relatively low, micro-cracks occur due to the inadequate liquid feeding during the solidification process. Under the condition that the volume fraction of liquid phase is sufficiently high, the interfacial cohesion between the grains and the liquid film is the determining factor that controls the tensile properties of the semisolid RAP processed alloys.

Author Contributions: J.F. designed most experiments, analyzed the results and wrote the manuscript. D.Y. performed most experiments and helped analyze the experimental data. K.W. gave some constructive suggestions about how to write the manuscript.

Acknowledgments: This research was funded by the Nation Natural Science Foundation of China [grant numbers 51174028, 51541406].

Conflicts of Interest: The authors declare no conflict of interest.

References

1. Balan, T.; Becker, E.; Langlois, L.; Bigot, R. A new route for semisolid steel forging. *CIRP Ann. Manuf. Technol.* **2017**, *66*, 297–300. [CrossRef]
2. Meng, Y.; Sugiyam, S.; Jun, Y. Microstructural evolution during partial melting and semisolid forming behaviors of two hot-rolled Cr–V–Mo tool steels. *J. Mater. Process. Technol.* **2015**, *225*, 203–212. [CrossRef]
3. Meng, Y.; Sugiyama, S.; Tan, J.; Yanagimoto, J. Effects of forming conditions on homogeneity of microstructure and mechanical properties of A6061 aluminum alloy manufactured bytime-dependent rheoforging on a mechanical servo press. *J. Mater. Process. Technol.* **2014**, *214*, 3037–3047. [CrossRef]
4. Rogal, Ł.; Dutkiewicz, J.; Atkinson, H.V.; Lityńska-Dobrzyńska, L.; Czeppe, T.; Modigell, M. Characterization of semisolid processing of aluminium alloy 7075 with Sc and Zr additions. *Mater. Sci. Eng.* **2013**, *580*, 362–373. [CrossRef]
5. Meng, Y.; Li, Q.; Tang, Y.; Sugiyama, S. Partial melting behaviors and thixoforming properties of cast and extruded Mg-5.15 Y-3.75 Gd-3.05 Zn-0.75 Zr alloys. *Vacuum* **2018**, *150*, 173–185. [CrossRef]
6. Jiang, J.F.; Chen, G.; Wang, Y. Compression mechanical behaviour of 7075 aluminium matrix composite reinforced with nano-sized SiC particles in semisolid state. *J. Mater. Sci. Technol.* **2016**, *32*, 1197–1203. [CrossRef]
7. Wang, L.; Qiu, F.; Zou, Q.; Yang, D.-L.; Tang, J.; Gao, Y.-Y.; Li, Q.; Han, X.; Shu, S.-L.; Chang, F.; et al. Microstructures and tensile properties of nano-sized SiCp/Al-Cu composites fabricated by semisolid stirring assisted with hot extrusion. *Mater. Charact.* **2017**, *131*, 195–200. [CrossRef]
8. Chen, G.; Chen, Q.; Qin, J.; Du, Z. Effect of compound loading on microstructures and mechanical properties of 7075 aluminum alloy after severe thixoformation. *J. Mater. Process. Technol.* **2016**, *229*, 467–474. [CrossRef]
9. Chen, Q.; Chen, G.; Ji, X.; Han, F.; Zhao, Z.; Wan, J.; Xiao, X. Compound forming of 7075 aluminum alloy based on functional integration of plastic deformation and thixoformation. *J. Mater. Process. Technol.* **2017**, *246*, 167–175. [CrossRef]
10. Jiang, J.F.; Atkinson, H.V.; Wang, Y. Microstructure and mechanical properties of 7005 aluminum alloy components formed by thixoforming. *J. Mater. Sci. Technol.* **2017**, *33*, 379–388. [CrossRef]
11. Rikhtegar, F.; Ketabchi, M. Investigation of mechanical properties of 7075 Al alloy formed by forward thixoextrusion process. *Mater. Des.* **2010**, *31*, 3943–3948. [CrossRef]
12. Kilicli, V.; Akar, N.; Erdogan, M.; Kocatepe, K. Tensile fracture behavior of AA7075 alloy produced by thixocasting. *Trans. Nonferr. Met. Soc. China* **2016**, *26*, 1222–1231. [CrossRef]
13. Rogal, Ł.; Dutkiewicz, J.; Góral, A.; Olszowska-Sobieraj, B.; Dańko, J. Characterization of the after thixoforming microstructure of a 7075 aluminium alloy gear. *Int. J. Mater. Form.* **2010**, *3*, 771–774. [CrossRef]
14. Wang, C.P.; Zhang, Y.Y.; Li, D.F.; Mei, H.S.; Zhang, W.; Liu, J. Microstructure evolution and mechanical properties of ZK60 magnesium alloy produced by SSTT and RAP route in semisolid state. *Trans. Nonferr. Met. Soc. China* **2013**, *23*, 3621–3628. [CrossRef]
15. Campo, K.N.; Proni, C.T.; Zoqui, E.J. Influence of the processing route on the microstructure of aluminum alloy A356 for thixoforming. *Mater. Charact.* **2013**, *85*, 26–37. [CrossRef]
16. Nayyeri, M.J.; Dehghani, K. Microstructure evolution in as-cast and SIMA-processed AE42 magnesium alloy. *J. Mater. Eng. Perform.* **2014**, *23*, 3077–3084. [CrossRef]
17. Bolouri, A.; Kang, C.G.; Shahmiri, M. Study on the effects of the compression ratio and mushy zone heating on the thixotropic microstructure of AA 7075 aluminum alloy via SIMA process. *J. Alloys Compd.* **2011**, *509*, 402–408. [CrossRef]
18. Bolouri, A.; Shahmiri, M.; Cheshmeh, E.N.H. Microstructural evolution during semisolid state strain induced melt activation process of aluminum 7075 alloy. *Trans. Nonferr. Met. Soc. China* **2010**, *20*, 1663–1671. [CrossRef]
19. Fu, J.L.; Wang, K.K.; Li, X.W.; Zhang, H.K. Microstructure evolution and thixoforming behavior of 7075 aluminum alloy in the semisolid state prepared by RAP method. *Int. J. Miner. Metall. Mater.* **2016**, *23*, 1404–1415. [CrossRef]
20. Arami, H.; Khalifehzadeh, R.; Keyvan, H.; Khomamizadeh, F. Effect of predeformation and heat treatment conditions in the SIMA process on microstructural and mechanical properties of A319 aluminum alloy. *J. Alloys Compd.* **2009**, *468*, 130–135. [CrossRef]

21. Mohammadi, H.; Ketabchi, M.; Kalaki, A. Microstructure evolution of semisolid 7075 aluminum alloy during reheating process. *J. Mater. Eng. Perform.* **2011**, *20*, 1256–1263. [CrossRef]
22. Liu, D.; Atkinson, H.V.; Kapranos, P.; Jirattiticharoean, W.; Jones, H. Microstructural evolution and tensile mechanical properties of thixoformed high performance aluminium alloys. *Mater. Sci. Eng. A* **2003**, *361*, 213–224. [CrossRef]
23. Bolouri, A.; Kang, C.G. Correlation between solid fraction and tensile properties of semisolid RAP processed aluminum alloys. *J. Alloys Compd.* **2012**, *516*, 192–200. [CrossRef]
24. Atkinson, H.V.; Burke, K.G.; Vaneetveld, G. Recrystallization in the semisolid state in 7075 aluminium alloy. *Mater. Sci. Eng. A* **2008**, *490*, 266–276. [CrossRef]
25. Binesh, B.; Aghaie, M. Phase evolution and mechanical behavior of the semisolid SIMA processed 7075 aluminum alloy. *Metals* **2016**, *6*, 42. [CrossRef]
26. Binesh, B.; Aghaie-Khafri, M. RUE-based semisolid processing: Microstructure evolution and effective parameters. *Mater. Des.* **2016**, *95*, 268–286. [CrossRef]
27. Manson-Whitton, E.D.; Stone, I.C.; Jones, J.R.; Grant, P.S.; Cantor, B. Isothermal grain coarsening of spray formed alloys in the semisolid state. *Acta Mater.* **2002**, *50*, 2517–2535. [CrossRef]
28. Annavarapu, S.; Doherty, R.D. Inhibited coarsening of solid-liquid microstructures in spray casting at high volume fractions of solid. *Acta. Metall. Mater.* **1995**, *43*, 3207–3230. [CrossRef]
29. Binesh, B.; Aghaie-Khafri, M. Microstructure and texture characterization of 7075 Al alloy during the SIMA process. *Mater. Charact.* **2015**, *106*, 390–403. [CrossRef]
30. Wang, Z.; Prashanth, K.G.; Scudino, S.; He, J.; Zhang, W.W.; Li, Y.Y.; Stoica, M.; Vaughan, G.; Sordelet, D.J.; Eckert, J. Effect of ball milling on structure and thermal stability of $Al_{84}Gd_6Ni_7Co_3$ glassy powders. *Intermetallics* **2014**, *46*, 97–102. [CrossRef]
31. Wang, Z.; Qu, R.T.; Scudino, S.; Sun, B.A.; Prashanth, K.G.; Louzguine-Luzgin, D.V.; Chen, M.W.; Zhang, Z.F.; Eckert, J. Hybrid nanostructured aluminum alloy with super-high strength. *NPG Asia Mater.* **2015**, *7*, e229. [CrossRef]
32. Wang, Z.; Qu, R.T. Compression behavior of inter-particle regions in high-strength $Al_{84}Ni_7Gd_6Co_3$ alloy. *Mater. Lett.* **2016**, *185*, 25–28. [CrossRef]
33. Chen, Q.; Zhao, Z.D.; Chen, G.; Wang, B. Effect of accumulative plastic deformation on generation of spheroidal structure, thixoformability and mechanical properties of large-size AM60 magnesium alloy. *J. Alloys Compd.* **2015**, *632*, 190–200. [CrossRef]
34. Jiang, J.F.; Wang, Y.; Atkinson, H.V. Microstructural coarsening of 7005 aluminum alloy semisolid billets with high solid fraction. *Mater. Charact.* **2014**, *90*, 52–61. [CrossRef]
35. Haghparast, A.; Nourimotlagh, M.; Alipour, M. Effect of the strain-induced melt activation (SIMA) process on the tensile properties of a new developed super high strength aluminum alloy modified by Al–5Ti–1B grain refiner. *Mater. Charact.* **2012**, *71*, 6–18. [CrossRef]
36. Chen, T.J.; Hao, Y.; Sun, J.; Li, Y.D. Effects of processing parameters on tensile properties and hardness of thixoformed ZA27 alloy. *Mater. Sci. Eng. A* **2004**, *382*, 90–103. [CrossRef]
37. German, R.M.; Suri, P.; Park, S.J. Review: Liquid phase sintering. *J. Mater. Sci.* **2009**, *44*, 1–39. [CrossRef]